Detailed black liquor drop combustion model for predicting fume in kraft recovery boilers

CHRISTOPHER L. VERRILL AND RICHARD A. WESSEL

ABSTRACT

Model predictions of sodium release from 2-mm black liquor drops were compared with results from two sets of experiments. The transient combustion model closely reproduces the sudden 5–20% sodium loss measured during drying and devolatilization, as well as the incremental loss during char burning. The amount and composition of fume was also accurately predicted for the combustion of 100-µm dried black liquor particles in an entrained-flow reactor operated at 700–1100°C with carrier gas containing 0–21% oxygen.

Application:

Engineers can assess the amount and composition of fume generated in recovery boilers by using mathematical models for the combustion of black liquor and the amount of alkali released.

MANY KRAFT RECOVERY BOILERS have difficulty in maintaining their design steam temperatures. Inorganic material builds up as deposits on surfaces that transfer heat by convection. Routine methods have not been effective at keeping these surfaces clean. As a result, gas passages can plug, which means costly downtime for intensive cleaning.

Recent experimental studies of aerosol formation, deposition, and removal have improved our fundamental understanding of boiler fouling and plugging. By incorporating mechanisms of aerosol formation in recovery boiler models, we can build an important tool for evaluating the effects that changes in boiler operation and design may have on fouling and plugging rates.

In this work, we modified a detailed model of the combustion of black liquor drops (*1*) to include important mechanisms of alkali release: physical ejection of material from burning particles, alkali chloride evaporation, and alkali carbonate reduction. These mechanims are considered to generate the submicron-sized fume that contributes to fouling and is collected in the electrostatic precipitator.

The model results of alkali release and fume formation were validated against laboratory data. Black liquor combustion and alkali release models were also implemented in B&W's three-dimensional furnace model to predict the amount and composition of aerosol generated at recovery boiler conditions (*2*).

BACKGROUND

There are four sources of the inorganic material that reaches the heat transfer surfaces:

1. Mechanical carryover of burning black liquor particles
2. Physical ejection of material from burning particles
3. Direct vaporization of alkali chlorides from burning particles and char deposits
4. Sodium and potassium vaporization from alkali carbonate reduction reactions in the char and smelt.

Mechanical carryover accounts for particles of 0.1–2.0 mm that enter the convective heat transfer zone. Physical ejection creates an aerosol fraction that consists of particles from 1 µm to 100 µm. The vaporization and condensation processes create a substantial amount of fume composed of submicron-sized particles.

Equilibrium models have been used to predict gaseous and particulate emissions from recovery boilers (*3–5*). This approach treats the furnace volume as one or more well-mixed chemical reactors. These models predict trends in fume formation, based on an average char bed temperature. However, they fall short of accounting for temperature nonuniformities, chemical reaction kinetics, and diffusion effects, which can significantly affect alkali vaporization rates. The main weakness of these models is that they rely on completely arbitrary factors to account for mechanical carryover and the release of liquor constituents during in-flight combustion.

Three-dimensional models have been developed to simulate turbulent flow, combustion, and heat transfer in kraft recovery boilers (*6–8*). Because thousands of particle trajectories can be tracked, these models can predict the entrainment of burning drops into heat transfer surfaces (mechanical carryover). A weakness of the three-dimensional models is that they cannot predict realistic dust loadings, as these predictions are based on estimates of mechanical carryover alone. The amount, size, and composition of fine aerosol must be taken into account to improve predictions of boiler fouling (*9*).

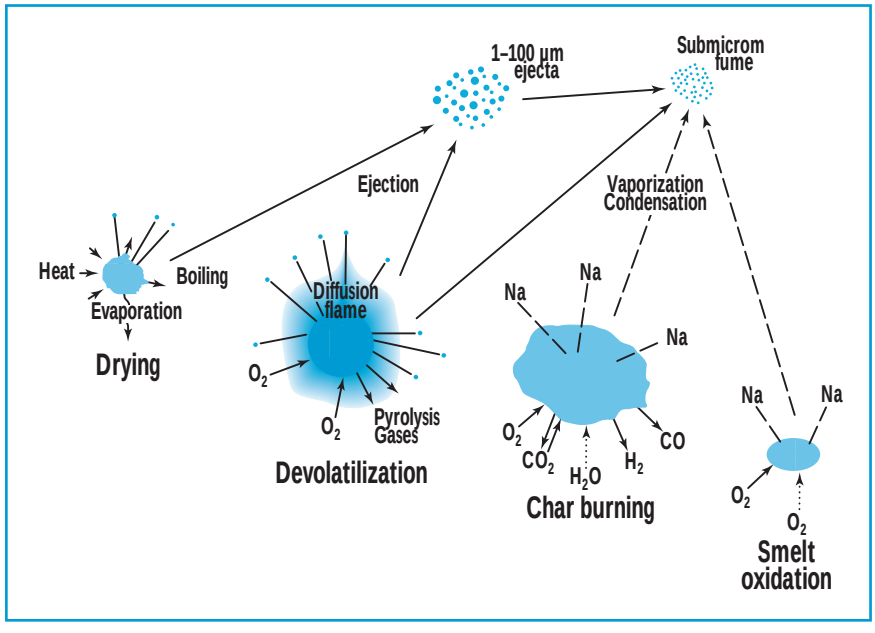

1. Black liquor drop combustion and inorganic aerosol formation processes taken into consideration for the model.

MODEL DESCRIPTION

A transient, one-dimensional model for black liquor drop combustion was previously developed to predict the heating rate and internal temperature gradients as a function of furnace temperature and particle size (*1*). The model accounts for drop aerodynamics, heat transfer, and chemical reaction. The particle position can be fixed in space with a cross flow of gas, as in a captive-drop furnace. Alternatively, the particle position and velocity can be permitted to vary, based on aerodynamic drag and gravitational forces, simulating a falling particle in an entrained-flow reactor or in a recovery boiler.

Particle mass and material component balances are solved for condensed species including water (H_2O), black liquor solids (BLS), fixed carbon ($C_{(s)}$), sulfate ($SO_4^=$), sulfide ($S^=$), carbonate ($CO_3^=$), sodium (Na^+), potassium (K^+), and chloride (Cl^-). Particle swelling behavior is characterized by a swelling factor which depends on the extent of drying, devolatilization, and char burning as described by Frederick (*10*). Porosity and bulk density are calculated along the particle trajectory based on the swelling factor and the remaining particle mass.

A multiple-resistance heat transfer model with 20–100 radial nodes or shells was chosen for this work to resolve the steep temperature gradients in the reacting particles. To improve the heat transfer model, we implemented experimentally determined radiation properties and the combustion of volatiles. Radiation properties were obtained from the measurement of spectral emittance of black liquor, char, and smelt (*11*). Homogeneous gas-phase combustion is simulated in the model when O_2 is present in the surrounding gases to react with volatiles and char combustion products (CO and H_2) that leave the particle. A one-dimensional diffusion flame envelopes the particle for small Reynolds numbers ($Re < 1$), assuming gas-phase reaction kinetics are infinitely fast and particles are well enough dispersed that particle-to-particle interactions may be neglected. The flame sheet radius and temperature are determined from an analytical solution of the one-dimensional transport equations for component chemical species and energy. The effect of the flame on convective heat and mass transfer to the particle surface is therefore predicted.

Figure 1 illustrates the stages of black liquor combustion and the alkali-release mechanisms considered in the model. Combustion is characterized in four stages: drying, devolatilization, char burning, and smelt oxidation. Drying and devolatilization occur very rapidly and are accompanied by particle swelling. Char burning is characterized by a number of heterogeneous chemical reactions that simultaneously consume carbon and reduce sodium sulfate to form liquid smelt. In the final stage, the smelt is reoxidized if oxygen is available. In the following sections, we describe the various alkali release mechanisms used to predict fume; details of the combustion models are given elsewhere (*1, 2*).

Physical ejection model

Single-drop experiments indicated that 5–20% of the sodium content of the black liquor is lost during the first seconds of exposure to hot gases (*12*). This loss appears to result from the physical ejection of liquor during drying and devolatilization. The extent of the loss increases with increasing initial drop size and laboratory furnace temperature. Water vapor and volatiles released within a reacting particle generate internal pressure, which causes the violent eruptions observed in captive-drop experiments (*13, 14*). Bits of liquor and char may be ejected with the escaping gases. In the model, physical ejection is assumed to occur during devolatilization.

$$BLS_{drop} \xrightarrow{R_{EJ}} BLS_{ejecta} \quad (1)$$

The composition of the ejected material is assumed to be the same as that of the black liquor particle at the time ejection occurs. The rate of physical ejection is proportional to the mass flow rate of water vapor

	Captive-drop furnace	Entrained-flow reactor
Gas temperature, °C	600	700
	700	800
	750	900
	800	1000
	900	1100
	1000	
Gas composition, % by vol.		
N_2	95	100
CO	5	0
Gas vertical velocity, m/s*	0.00	-0.23
	0.61	-0.26
	1.83	-0.28
	-0.30	
	-0.33	
Particle residence time, s	0–60	0.80
		0.75
		0.70
		0.65
		0.60

*Positive values indicate upward velocities.

I. Furnace conditions used as model inputs

	Captive-drop furnace	Entrained-flow reactor
INITIAL DROP CONDITIONS		
Solids, %	70	100
Temperature, °C	115	115
Density, g/cm³	1.380	1.566
Diameter, mm	2.0	0.1
Vertical velocity, m/s*	0	-0.214
BLACK LIQUOR SOLIDS		
Elemental comp., % by wt.		
Carbon	37.8	34.9
Hydrogen	3.60	3.05
Nitrogen	0	0
Sulfur	5.4	2.9
Sodium	19.30	22.65
Potassium	1.00	0.62
Chlorine	0.40	0.67
Oxygen	32.50	35.21
Higher heating value, kJ/kg	14,500	13,000
DEVOLATILIZATION PARAMETERS		
Carbon yield	0.40	0.53
Sulfur yield	0.35	0.35
Initial char sulfate reduction	0.54	0.54
VOLUMETRIC SWELLING FACTORS		
Drying	3.375	1
Devolatilization	27	27

*Positive values indicate upward velocities.

II. Initial drop conditions and black liquor combustion parameters used as model inputs

and volatile gases if the internal pressure drop exceeds a critical value:

$$R_{EJ} = A_{EJ}(R_{H_2O} + \alpha_{VL} R_{BLS}) \quad (2)$$

if

$$\Delta P_{max} > \frac{(\Delta P d_p)_{EJ}}{d_p}$$

The formulation of the rates of drying, R_{H_2O}, and of devolatilization, R_{BLS}, is presented elsewhere (*1*). The critical pressure is related to drop diameter in the above inequality to approximate the effect of particle size, assuming that physical ejection is negligible below an initial drop size of 0.2 mm. The rate coefficient, A_{EJ}, and the internal pressure drop parameter, $(\Delta P\ d_p)_{EJ}$, were chosen to fit measurements of initial sodium loss made earlier (*12*).

The internal pressure of the particle drop is calculated from correlations for flow through a porous medium (*15*). Assuming that viscous resistance is much larger than inertial resistance, then the latter can be neglected. The mass flow rate of water vapor and volatile gases is calculated as a function of radius within the particle volume. The pressure drop from the center of the porous sphere to the surface is given by:

$$\Delta P = \int_0^r \alpha \mu_g V dr = \int_0^r \frac{\alpha \mu_g \dot{m}_g}{4\pi \rho_g r^2} dr \quad (3)$$

where μ_g is the gas viscosity, V is the superficial gas velocity, and α is the viscous resistance coefficient. In the second equality, the superficial velocity is replaced by the mass flow rate of water vapor and volatile gases, $\dot{m}_g$, and the gas density, ρ_g. The viscous resistance coefficient, α, is approximated using an expression from Ergun (*16*) for packed beds:

$$\alpha = A \frac{(1-\varepsilon)^2}{\varepsilon^3 \delta^2} \quad (4)$$

where ε is the porosity, A = 150 as an empirical constant, and $\delta = 10^{-5}$ m as the assumed pore size.

Temp., °C	Gas velocity m/s	Predicted beginning of devolatilization, s	Measured onset of swelling, s	Predicted end of drying, s	Predicted MSV, s	Measured MSV, s
600	0.61	0.82	3.8 ± 0.6	5.48	6.25	6.4 ± 1.0
750	0.61	0.39	1.9 ± 0.2	3.51	3.62	3.2 ± 0.3
750	1.83	0.30	1.9 ± 0.2	3.11	3.21	3.2 ± 0.3
900	0.61	0.22	1.2 ± 0.2	2.30	2.33	2.3 ± 0.4

III. Comparison of measured and predicted drop combustion times

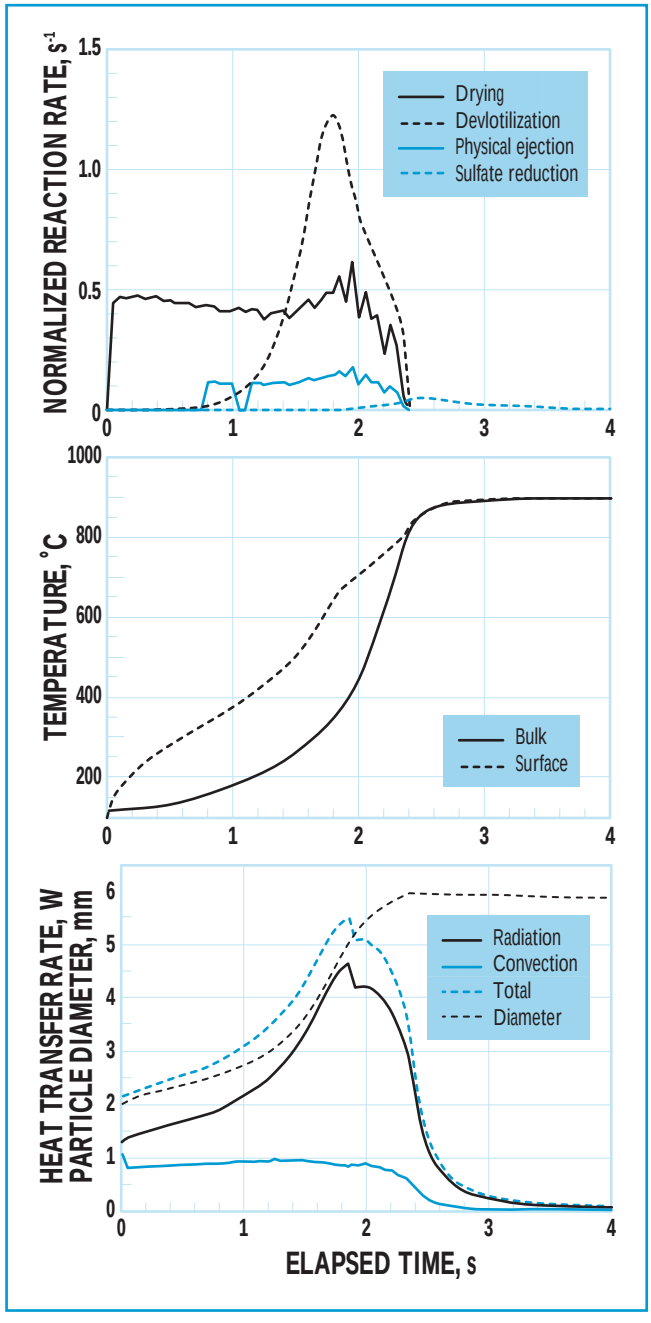

2. Predicted behavior for a 2-mm captive drop during exposure time (70% initial solids in 95% N_2 with 5% CO at 900°C, at a gas velocity of 0.61 m/s). (The one-to-one correspondence was coincidental between the heating rate scale in watts and the diameter scale in millimeters.)

Model for alkali carbonate reduction

During char burning, sodium and potassium carbonate (collectively referred to as M_2CO_3) are reduced by char carbon to produce alkali vapor, CO and CO_2.

$$C_{(s)} + (2-f)M_2CO_{3(l,s)} \xrightarrow{\hat{R}_{C/CO_3}} 2(2-f)M_{(g)} + fCO_{(g)} + (3-2f)CO_{2(g)} \qquad (5)$$

The variable stoichiometry indicated by the use of the parameter *f* reflects the fact that both CO and CO_2 are products of the reaction.

The reduction of alkali carbonate is potentially an important mechanism for char carbon removal and an important source of the submicron aerosol. The rate of alkali vaporization is controlled by the kinetics of the M_2CO_3 reduction. Experimental results suggest the reaction is inhibited by CO and CO_2 (*17*); however, an approach for modeling the reaction-suppressing effects of CO and CO_2 has not been developed. In the absence of mass transfer resistance terms, a first-order dependence on char carbon is assumed to limit the rate of M_2CO_3 reduction in order to be consistent with experimental measurements.

$$\hat{R}_{C/CO_3} = \frac{m}{(2-f)} k\rho\left[C_{(s)}\right]\left[CO_3^{=}\right]\exp\left(-E/R_u T\right) \qquad (6)$$

where $k = 1.0 \times 10^9$ m³/kgmol·s, $E = 2.44 \times 10^8$ J/kgmol, and *m* is the mass remaining in the reacting particle. The brackets denote concentration in kgmol/kg.

Alkali chloride vaporization model

The vapor pressures of NaCl and KCl become appreciable at temperatures above 900°C, and these alkali chlorides are assumed to vaporize directly from black liquor char and smelt (*18*):

$$MCl_{(s,l)} \xrightarrow{\hat{R}_{MCl}} MCl_{(g)} \qquad (7)$$

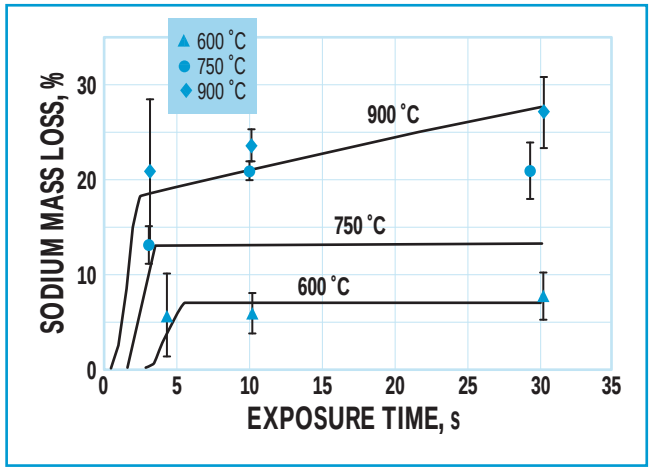

3. Measured and predicted sodium loss for 2-mm captive drops in the IPST flow reactor. (Measurements are indicated by points with error bars.)

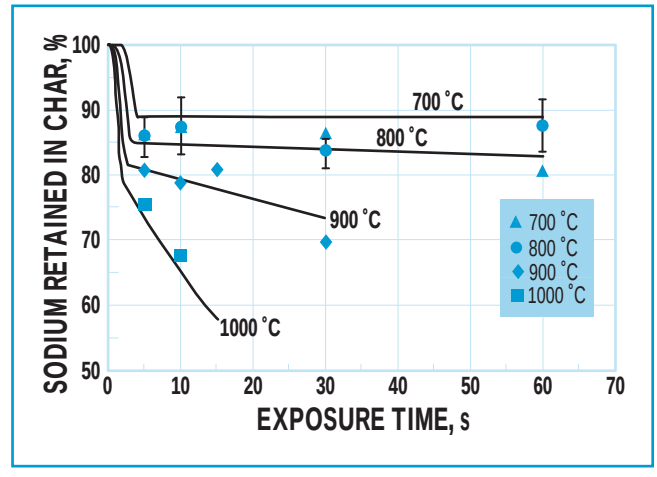

4. Measured and predicted sodium loss for 2-mm captive drops in the Åbo Akademi muffle furnace. (Measurements are indicated by points with error bars.)

Assuming the evaporation rate is controlled by convective mass transport of vapor from the boundary layer, then the molar flux of species *i* is:

$$\hat{R}_i = H_{m,i} A_S \left(C_i^S - C_i^\infty \right) \qquad (8)$$

where *i* is NaCl or KCl and A_s is the surface area of the particle. The molar vapor concentrations at the surface C_i^S and at freestream conditions C_i^∞ are determined by a multi-phase equilibrium calculation. The convective mass transfer coefficient $H_{m,i}$ is calculated from empirical relationships similar to those for convective heat transfer and based on diffusion coefficients of alkali chloride vapors.

Prediction of fume from black liquor combustion

The 1–100-µm particles that are ejected from large black liquor drops react quickly and are easily entrained by the gas. These particles are assumed to dry and devolatilize instantaneously. Due to their small size and large surface area, it is assumed that ejected particles are at the gas temperature and that char burning is dominated by heterogeneous reactions with CO_2, H_2O, and O_2. Sulfate and carbonate reduction reactions within the ejected particles are neglected. The fate of the ejected material at recovery boiler conditions is unknown. Presumably, for a significant fraction of inorganics in the particles, inorganic compounds are vaporized and thus contribute to submicron aerosol formation.

The mass of inorganic aerosol predicted by the model includes the Na, K, and Cl released during black liquor combustion, plus the inorganic material from ejecta particles, plus the C, H, S, and O in the gas that combine with these elements. The composition of the inorganic species includes Na, NaCl, NaOH, Na_2S, Na_2SO_4, Na_2CO_3, K, KCl, KOH, K_2S, K_2SO_4, and K_2CO_3, which may be in the form of gas (vapor) or liquid and solid aerosol. The model does not currently take into account the aerosol particle size distribution.

RESULTS AND DISCUSSION

Single-particle model predictions of combustion rates and alkali release were validated with laboratory data taken at Åbo Akademi University (ÅAU), the Institute of Paper Science and Technology (IPST), and Oregon State University (OSU). The furnace conditions and combustion parameters used as model inputs are summarized in **Tables I and II**.

2-mm Captive drops

Sodium release was predicted for pyrolysis of 2-mm black liquor drops, and results were compared with data from captive-drop experiments. The captive-drop experiments were conducted to determine the relative change in sodium content of black liquor as a function of furnace temperature and exposure time. A muffle furnace apparatus with no forced convection was utilized for the experiments at ÅAU (*19*), and a tube furnace with a relative gas velocity of 0.61–1.83 m/s was employed at IPST (*12*).

In both sets of experiments, individual drops of the industrial black liquors were formed on a fine wire and were inserted into the laboratory furnace. These drops averaged 2 mm in initial diameter and had an initial solids content about 70%. After 3–60 s exposure to a pyrolytic environment (95% N_2 with 5% CO), the char was withdrawn and quenched with nitrogen gas. The change in sodium content was then determined as described elsewhere (*12*). Timed observation of drop behavior in the furnace was recorded on video tape, and characteristic combustion times were determined.

The combustion-stage times calculated by the single drop model are compared to measured values in **Table III** for several conditions in the IPST furnace. While it is not possible to identify the beginning and ending points of drying and devolatilization from captive-drop experiments, the times to the onset of swelling and

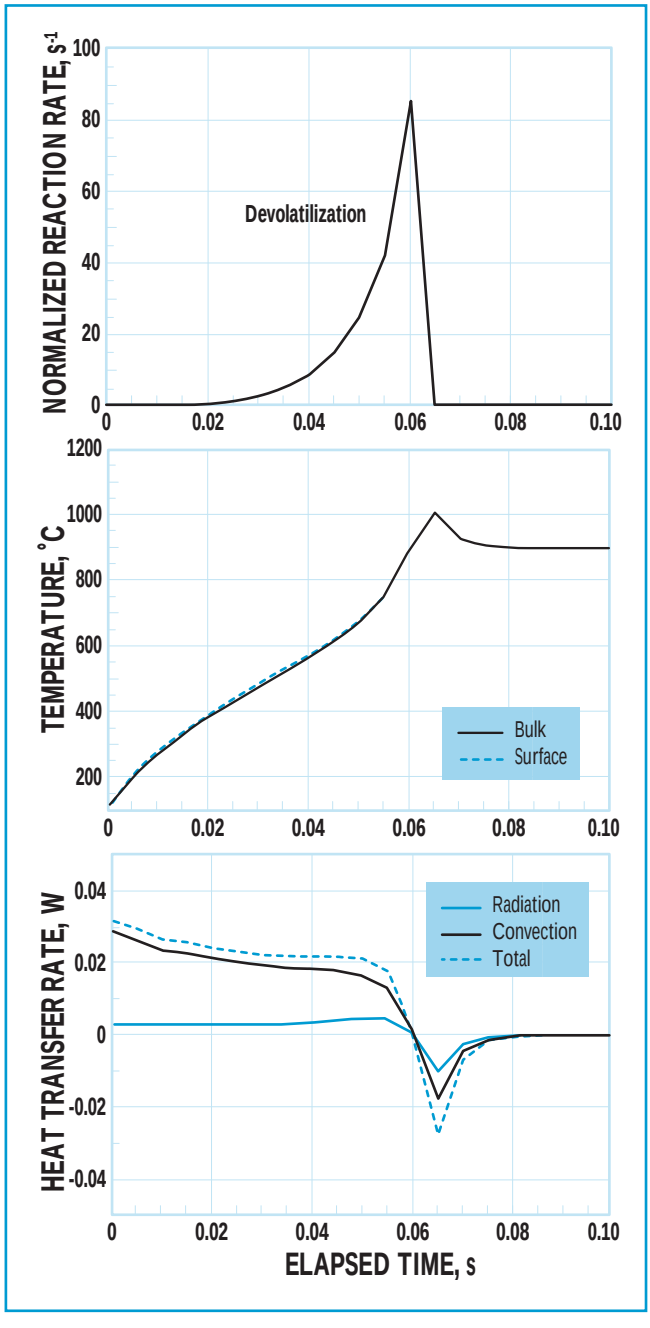

5. Predicted behavior for a 100-µm falling particle during exposure time (100% initial solids in 100% N_2 at 900°C, at a gas velocity of –0.28 m/s).

maximum swollen volume (MSV) can be precisely measured. A parameter for internal radiative heat transfer was adjusted to provide the best fit with experimental times to MSV (*1*). Modeling parameters were then held constant for all other simulations. In view of the range of experimental variability, the model accurately predicts the time to MSV for captive drops in a flowing, noncombustive gas. The onset of swelling, determined from the video images, falls between the predicted beginning of devolatilization and the end of drying.

In **Fig. 2**, the top graph shows predicted reaction rates for the pyrolysis of a 2-mm captive drop at 900°C. Drying, devolatilization, and sulfate reduction rates are normalized by the initial mass of water, black liquor solids, and fixed carbon, respectively. Physical ejection rate is normalized by the initial mass of black liquor solids in the particle. The plotted reaction rates show that the stages of drying and devolatilization are not distinct but that they overlap significantly as a result of steep temperature gradients within the particle. The center of the particle is still drying at the black liquor saturation temperature while the outside layers are undergoing devolatilization and char burning. This result is consistent with observations of overlapped combustion stages in the IPST reactor (*14*).

Predictions of heat transfer rate in the lowest graph in Fig. 2 suggest that radiation is the most significant mode of transferring heat to the particle surface for large drops. Heat transfer increases significantly with surface area as the particle swells to MSV, then decreases to zero as the particle approaches the furnace temperature. The particle becomes uniform in temperature after about 2.3 s, when devolatilization is complete (middle graph).

Experimental results of loss in sodium mass from the IPST reactor were reported as percentages of the initial sodium content of liquor solids. Measured and predicted values are compared in **Fig. 3**. The experimental results indicated that a sodium loss of 5.7–21.0% occurred at the shortest residence time investigated, near the point of MSV. For pyrolysis at 600°C, there is no further sodium release after the rapid loss of 5.7% of the initial sodium content. At temperatures of 750°C and above, sodium loss does not subside but continues to increase with exposure time. The initial sodium loss is expected to result from the physical ejection of liquor and char during drying and devolatilization. In the second phase of sodium loss, the loss occurs at a much lower rate than during the initial release and is presumed to result from Na_2CO_3 reduction by char carbon (*17*). The measurements indicate that CO may have a role in suppressing this sodium loss at 750°C, because the rate of loss decreases and then levels out after 10 s of exposure time. At 900°C, the presence of CO in the gas atmosphere is not sufficient to completely prevent Na_2CO_3 reduction by char carbon, as indicated by the increase in sodium loss between 10 s and 30 s.

Constants in the physical ejection model, A_{EJ} and $(\Delta P\, d_p)_{EJ}$, were adjusted to provide the best fit with the initial sodium loss data from the IPST experiments. Modeling parameters were then held constant for all other simulations. Predicted values demonstrate the initial phase of sodium loss seen in the data and exhibit the same slope as do the experimental results within the range of exper-

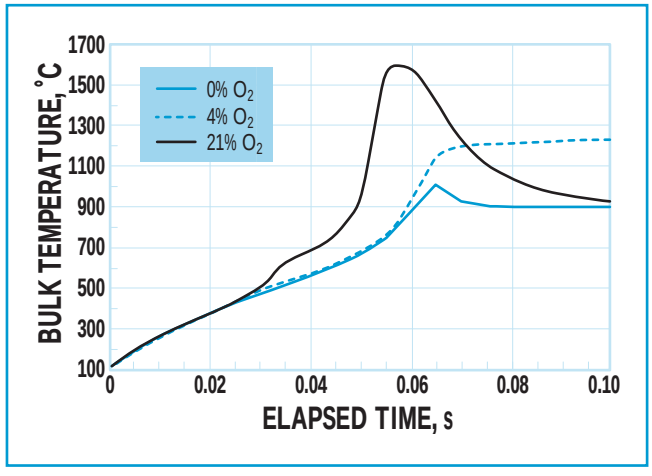

6. Predicted effect of oxygen on bulk temperature of a 100-µm falling particle over the exposure time (100% initial solids in 100% N_2 at 900°C, –0.28 m/s gas velocity).

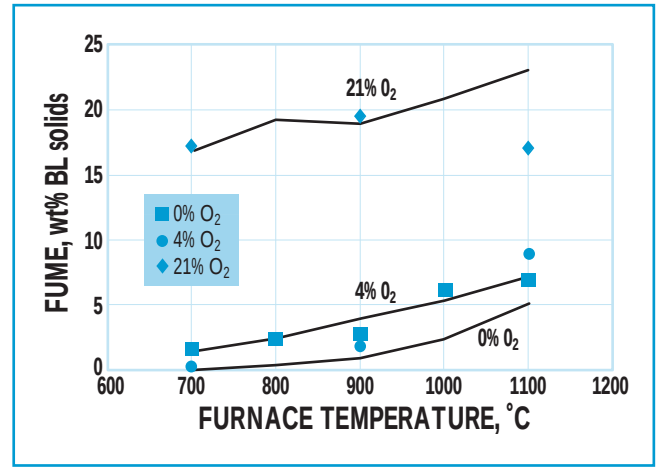

7. Measured and predicted fume yield for 100-µm particles in the OSU entrained-flow reactor. (Measurements are indicated by points.)

imental uncertainty. The model does not reproduce the 750°C data at 10 s and 30 s accurately; however, the changes in sodium release rates observed in the data cannot be fully explained (*12*). The presence of CO has no effect on the predicted trends because terms for CO and CO_2 suppression are not included in the model (Eq. 6).

The results of the ÅAU experiments were reported as percentages of sodium retained in the char; measured and predicted values are compared in **Fig. 4**. These data exhibit the same trends as the data of Verrill *et al.* (*12*). Analysis of the experimental results indicates that there is a rapid sodium loss of 14–18% prior to the end of devolatilization (*19*). For temperatures above 800°C, sodium loss does not subside but continues to increase with exposure time, though at a much lower rate than the initial release. Once again, predicted values accurately reproduce the initial phase of sodium loss seen in the data and exhibit the same slope as the experimental results exhibit within the range of experimental uncertainty.

100-µm entrained particles

Fume formation was predicted for combustion of 100-µm dried black liquor particles, and results were compared with data from the OSU laminar entrained-flow reactor (*20*). These experiments used dry black liquor solids, 90–125 µm, in nitrogen with 0% 0_2, 4% O_2, and 21% O_2 environments at furnace temperatures ranging from 700°C to 1100°C. The particle heating rate was of the order of 10^4 to 10^5 °C/s, and the residence time was 0.6–0.8 s. The samples were quenched to stop the reactions, and solid products of combustion were collected as char (larger than 3 µm) and fine particles (smaller than 3 µm). Reis *et al.* (*20*) did not measure combustion times, swollen volumes, and particle temperatures. Table II gives the elemental composition of dry black liquor solids used in the experiments and in the model.

In **Fig. 5**, the top graph shows predicted reaction rates for pyrolysis of a 100-µm falling particle at 900°C in the OSU entrained-flow reactor. Devolatilization is the only reaction rate that appears in the plot because there is no initial water content and because no appreciable sulfate reduction occurs in the first 0.1 s of exposure time. Note that devolatilization is completed quickly (0.061 s) compared to the residence time when the solid products are collected (0.70 s).

In contrast to the middle graph of Fig. 2 for the large drops, the middle graph of Fig. 5 suggests the temperature is nearly uniform within the fine particle. The particle temperature exceeds the furnace temperature near the end of devolatilization because devolatilization is slightly exothermic in the model. The model predicts that convection is the most significant mode of heat transfer to the particle surface (lowest graph, Fig. 5). Heat transfer is initially positive as the particle heats up, but it becomes negative when the particle exceeds the furnace temperature, and then it approaches zero as the particle cools to the furnace temperature.

Addition of oxygen to the carrier gas results in the homogeneous combustion of volatiles and char burning products (H_2 and CO), and the surrounding flame elevates the particle temperature above that of the furnace. This temperature rise has been measured for 1–3-mm captive drops over a range of oxygen contents (*21*). With experimental measurements lacking for fine particles in the OSU entrained-flow reactor, the model was used to determine trends in particle temperature as a function of oxygen content (**Fig. 6**). A temperature rise of approximately 300°C during char burning is predicted when 4% O_2 is added to the nitrogen carrier gas. The particle temperature returns to 900°C at the end of char burning (0.125 s); however, this change is not shown in the time scale of Fig. 6. In air at 900°C, the model predicts that escaping

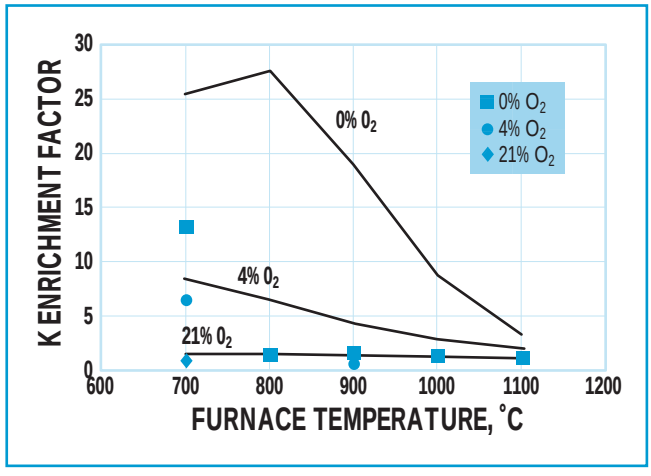

8. Measured and predicted potassium enrichment for 100-µm particles in the OSU entrained-flow reactor. (Measurements are indicated by points.)

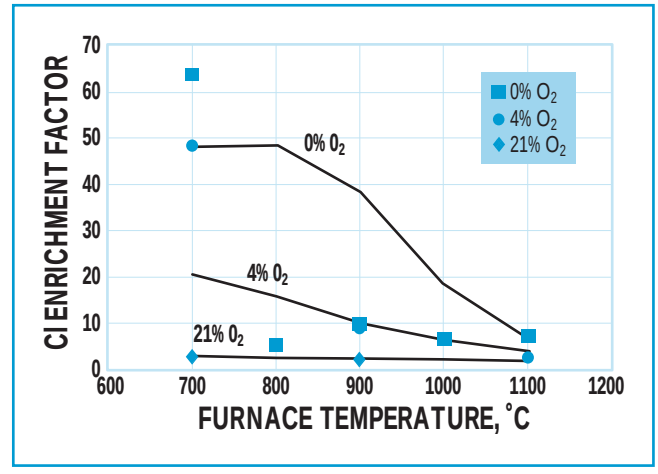

9. Measured and predicted chloride enrichment for 100-µm particles in the OSU entrained-flow reactor. (Measurements are indicated by points.)

volatiles ignite after 0.03 s and cause an initial temperature rise. A steep increase to 1581°C then takes place because char oxidation is occurring at the particle surface under these highly oxidizing conditions. The char burning rate increases with temperature, and carbon is rapidly consumed. By 0.06 s, the fully oxidized inorganic residue has begun cooling to the furnace temperature.

Measured and predicted fume yields are compared in **Fig. 7**. The predicted quantity of fume from the OSU experiments increases with both the reactor temperature and oxygen concentration because the rate of alkali carbonate reduction increases strongly with particle temperature (Eq. 6). There is generally good agreement between experimental and model results; however, the data show no clear difference between the quantity of submicron aerosol collected at 0% and 4% O_2 content and no distinct trend with furnace temperature at 21% O_2. We believe the reported values of inorganic fume at 0% O_2 are too high, because there was a significant amount of soot collected in the fine particle fraction at all temperatures (13–42% by weight). Reis *et al.* (*20*) explain that the reported values for fume were corrected by subtracting the mass of fixed carbon. However, the fine material collected at 4% and 21% O_2 contained no soot, and the values were not subject to errors introduced by correcting for the mass of carbon. The apparent decrease in measured fume yield at 1100°C and 21% O_2 may result from a limitation in the experimental method. The amount of fume generated at these conditions of maximum particle temperature exceeds the capacity of the filter used to collect the fine particulate (*22*). The total fume generated by combustion in air is expected to increase with furnace temperature as predicted by the model.

Potassium and chloride enrichment are defined as the relative amounts of potassium and chlorine in the fume, using total alkali as the basis, compared to that in the initial black liquor solids (BLS):

$$\text{Potassium enrichment factor} = \frac{[K/(Na+K)]_{fume}}{[K/(Na+K)]_{BLS}} \quad (9)$$

$$\text{Chloride enrichment factor} = \frac{[Cl/(Na+K)]_{fume}}{[Cl/(Na+K)]_{BLS}} \quad (10)$$

Predicted potassium enrichment (**Fig. 8**) and chloride enrichment (**Fig. 9**) decrease with temperature and oxygen concentration because the effect of particle temperature is much greater on M_2CO_3 reduction (Eq. 5) than on MCI vaporization (Eq. 7). The increasing amount of alkali vapor dilutes the relatively limited amount of chloride vapor as particle temperature increases. Therefore, increasing the oxygen content has essentially the same effect as increasing the furnace temperature: it increases Na_2CO_3 reduction and reduces measured and predicted K and Cl enrichments. The predicted trends are reasonably accurate in view of experimental uncertainty; for example, the data taken at 0% O_2 are subject to uncertainty caused by soot formation.

Effect of particle size on the extent of physical ejection

The residence time in the OSU reactor is 5–10 times longer than the time required for devolatilization; therefore, it is not possible to determine if physical ejection occurred during the OSU experiments. However, a comparison of the experimental results at 900°C for pyrolysis of a 2-mm drop (Fig. 4) and a 100-µm entrained particle (Fig. 7) suggests that physical ejection of material is negligible for the fine particles.

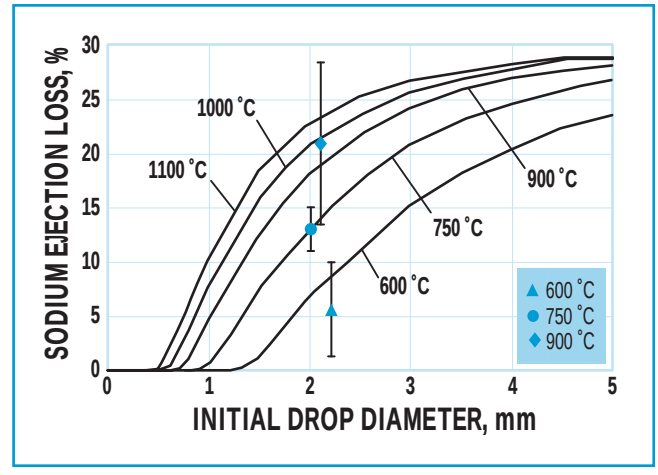

10. Effect of drop size on the predicted physical ejection yield. (Data from the IPST 2-mm captive drop experiment are indicated by points with error bars.)

Without a consistent set of experimental data taken at various drop sizes, the model was used to extrapolate the effect of drop size on physical ejection yield for realistic spray combustion conditions. In **Fig. 10**, the predictions for pyrolysis of IPST liquor over a range of drop sizes and a range of furnace temperatures are compared with the initial sodium loss from Verrill *et al.* (*12*).The model predicts that the trends with increasing drop size and temperature converge toward a maximum physical ejection yield of about 30%. These results suggest that reducing the median drop size or redistributing the liquor to a cooler zone of the furnace could affect a reduction in physical ejection and consequently in the formation of fume. However, the effects of drop size need to be confirmed experimentally before substantial conclusions can be drawn from the model.

CONCLUSIONS

A detailed model for black liquor drop combustion and alkali release has been developed and validated with laboratory data for 2-mm captive drops and 100-µm entrained particles. This model provides valuable insights needed to understand drying, devolatilization, and char burning processes, as well as the associated sodium loss quantities.

Limited laboratory results suggest that physical ejection of material during black liquor drop combustion may be the most significant source of recovery boiler aerosol.The phenomenon of pressure-induced microexplosions from escaping water vapor and volatile gases is the proposed mechanism presumed to control alkali release during drying and devolatilization, and a suitable model was developed to describe this process. To model spray combustion conditions more realistically will require additional experiments to measure physical ejection yield over a range of initial drop sizes and solids contents.

Laboratory experiments suggest that alkali carbonate reduction is a significant source of submicron aerosol at long residence times and high temperatures. According to full-scale model predictions (*2*), the char bed of a recovery boiler produces more fume by this mechanism than do entrained particles. Before this reaction can be modeled at actual combustion conditions, additional experiments are needed. These experiments will have to quantify the role of fixed carbon on alkali carbonate reduction and elucidate the reaction-suppressing effects of CO and CO_2.

Engineers need the ability to predict the amount and composition of fume and mechanical carryover if they are to evaluate accurately the fouling and plugging of convective surfaces in recovery boilers. As reported here, combustion and alkali-release models have been implemented in a three-dimensional furnace model to predict aerosol dust loadings in several recovery boilers. The validation of these predictions with boiler test data is reported elsewhere (*2*).

Important advances in modeling aerosol nucleation, growth, and deposition have been reported by Jokiniemi *et al.* (*23*). However, their simplistic alkali release models cannot predict the effect of boiler operating conditions on the amount and composition of the carryover and aerosol entering the heat transfer surfaces. Coupling good alkali release and aerosol dynamics models in a three-dimensional model should substantially improve our ability to predict fouling and plugging in kraft recovery boilers.TJ

Verrill is a research engineer and Wessel is a principal engineer in the Research and Development Division of McDermott Technology, Inc. (formerly of Babcock & Wilcox Company), 1562 Beeson St., Alliance, OH 44601.

Received for review Nov. 22, 1996.
Accepted Oct. 11, 1997.

Presented at the 1997 Pulping Conference.

NOMENCLATURE

A_s = particle surface area, m²
BLS = black liquor solids
C_i^s = molar concentration of gas species *i* at the particle surface, kgmol/m³ gas
C_i^∞ = molar conc. of gas species *i* in bulk gas, kgmol/m³ gas
d_p = particle diameter, m
E = activation energy, J/kgmol
f = stoichiometric coefficient for CO in carbonate reduction products, kgmol CO/kgmol C
$H_{m,i}$ = convective mass transfer coefficient for species *i*, m/s
k = chemical kinetic rate constant, m³/kgmol·s
m = particle mass, kg
$\dot{m}_g$ = mass flow rate of water vapor and volatiles, kg/s
M = generalized alkali element, Na or K
r = particle radius, m
R_{H_2O} = mass reaction rate of drying, kg H_2O per second
R_{BLS} = mass reaction rate of devolatilization, kg BLS/s
R_{EJ} = mass reaction rate of physical ejection, kg BLS/s
R_u = universal gas constant, 8314.3 J/kgmol·K
$\hat{R}_{C/CO_3}$ = molar reaction rate of carbon by alkali carbonate reduction, kgmol C/s
$\hat{R}_{MCl}$ = molar evaporation rate of alkali chloride, kgmol MCl/s
T = char temperature, K
V = superficial gas velocity, m/s
$[C_{(s)}]$ = molar concentration of carbon, kgmol $C_{(s)}$/kg solid
$[CO_3^=]$= molar concentration of carbonate, kgmol $CO_3^=$/kg solid
α_{VL} = volatile gas yield, kg volatiles/kg BLS
ΔP = change in internal pressure of liquor drop or particle, N/m²
ε = char porosity
μ_g = gas molecular viscosity, kg/m·s
ρ = char density, kg/m³
ρ_g = gas density, kg/m³

LITERATURE CITED

1. Verrill, C. L. and Wessel, R.A., *CPPA 1995 International Chemical Recovery Conference Proceedings*, Technical Section CPPA, Montreal, p. B89.
2. Wessel, R.A. and Verrill, C. L., *TAPPI 1996 Engineering Conference Proceedings*, TAPPI PRESS, Atlanta, p. 775.
3. Bhada, R. K., Lange, H. B., and Markant, H. P., *TAPPI 1972 Environmental Conference Proceedings*, TAPPI PRESS, Atlanta, p. 5.
4. Pejryd, L. and Hupa, M., *TAPPI 1984 Pulping Conference Proceedings*, TAPPI PRESS, Atlanta, p. 579.
5. H.-Kochesfahani, S., Tran, N. H., Tavares, A., *et al.*, *82nd Technical Section CPPA Proceedings*, 1996, Technical Section CPPA, Montreal, p. B279.
6. Grace, T., Walsh, A., Jones, A., *et al.*, *CPPA 1989 International Chemical Recovery Conference Proceedings*, Technical Section CPPA, Montreal, p. 1.
7. Nowak, P., Matys, P., Sabhapathy, P., *et al.*, *CPPA 1995 International Chemical Recovery Conference Proceedings*, Technical Section CPPA, Montreal, p. A149.
8. Wessel, R. A., Parker, K. L., and Verrill, C. L., *TAPPI J.* 80(10): 207(1997).
9. Grace, T. M., *Tappi J.* 79(7): 182(1996).
10. Frederick, W. J., *Combustion Processes in Black Liquor Recovery: Analysis and Interpretation of Combustion Rate Data and an Engineering Design Model*, Report No. 1, U.S. Dept. of Energy, DOE/CE/40637-T8 (DE90012712) (March, 1990).
11. Wessel, R. A. and Bailey, R. T., *Radiative Heat Transfer Properties for Black Liquor Combustion*, Final Project Report Apr. 1, 1995– Aug. 30, 1996, Subcontract No. 1 between IPST and Babcock and Wilcox, DOE DE-FG02-90CE40936 (August 27, 1996).
12. Verrill, C. L., Grace, T. M., and Nichols, K. M., *J. Pulp Paper Sci.* 20(12): J354(1994).
13. Hupa, M., Solin, P., and Hyöty, P., *J. Pulp Paper Sci.* 13(2): J67(1987).
14. Verrill, C. L. and Nichols, K. M., *AIChE Symp. Ser.* 90(302): 55(1994).
15. Perry, R. H. and Green, D. *Chemical Engineers' Handbook*, 6th edition, McGraw-Hill, p. 5–56, 1984.
16. Ergun, S., *Chem. Eng. Prog.* 48(2): 89(1952).
17. Li, J. and van Heiningen, A. R. P., *Tappi J.* 73(12): 213(1990).
18. Cameron, J. H., *J. Pulp Paper Sci.* 14(4): J76(1988).
19. Frederick, W. J., Forssén, M., Hupa, M., *et al.*, *TAPPI 1992 International Chemical Recovery Conference Proceedings*, TAPPI PRESS, Atlanta, p. 599.
20. Reis, V.V., Frederick W. J., Wåg, K. J., *et al.*, *Tappi J.* 78(12): 67(1995).
21. Frederick, W. J., Hupa, M., Stenberg J., *et al.*, *Fuel* 73(12): 1889(1994).
22. Frederick, W. J., personal communication (Nov. 11, 1996).
23. Jokiniemi, J. K., Pyykönen, J., Mikkanen, P., *et al.*, *TAPPI J.* 79(7): 171(1996).